Atmos. Chem. Phys. Discuss., 9, 7115–7154, 2009
www.atmos-chem-phys-discuss.net/9/7115/2009/

Atmospheric Chemistry and Physics Discussions

This discussion paper is/has been under review for the journal *Atmospheric Chemistry and Physics (ACP)*. Please refer to the corresponding final paper in *ACP* if available.

Kinetics and mechanisms of heterogeneous reaction of NO_2 on $CaCO_3$ surfaces under dry and wet conditions

H. J. Li, T. Zhu, D. F. Zhao, Z. F. Zhang, and Z. M. Chen

State Key Joint Laboratory of Environmental Simulation and Pollution Control, College of Environmental Sciences and Engineering, Peking University, Beijing, 100871, China

Received: 7 January 2009 – Accepted: 30 January 2009 – Published: 17 March 2009

Correspondence to: T. Zhu (tzhu@pku.edu.cn)

Published by Copernicus Publications on behalf of the European Geosciences Union.

Abstract

Calcium nitrate ($Ca(NO_3)_2$) was observed in mineral dust and could change the hygroscopic and optical properties of mineral dust significantly due to its strong water solubility. The reaction of calcium carbonate ($CaCO_3$) with nitric acid (HNO_3) is believed the main reason for the observed $Ca(NO_3)_2$ in the mineral dust. In the atmosphere, the concentration of nitrogen dioxide (NO_2) is orders of magnitude higher than that of HNO_3; however, little is known about the reaction of NO_2 with $CaCO_3$. In this study, the heterogeneous reaction of NO_2 on the surface of $CaCO_3$ particles was investigated using diffuse reflectance infrared Fourier transform spectroscopy (DRIFTS) combined with X-ray photoelectron spectroscopy (XPS) and scanning electron microscopy (SEM) under wet and dry conditions. Nitrate formation was observed in both conditions, and nitrite was observed under wet conditions, indicating the reaction of NO_2 on the $CaCO_3$ surface produced nitrate and probably nitrous acid (HONO). Relative humidity (RH) influenced both the initial uptake coefficient and the reaction mechanism. With RH<52%, surface –OH was formed through dissociation of the surface adsorbed water via oxygen vacancy, thus determining the reaction order. With RH>52%, a monolayer of water formed on the surface of the $CaCO_3$ particles, which reacted with NO_2 as a first order reaction, forming HNO_3 and HONO. The initial uptake coefficient γ_0 was determined to be $(1.66\pm0.38)\times10^{-7}$ under dry conditions and up to $(0.84\pm0.44)\times10^{-6}$ under wet conditions. Considering that NO_2 concentrations in the atmosphere are orders of magnitude higher than those of HNO_3, the reaction of NO_2 on $CaCO_3$ particle should have similar importance as that of HNO_3 in the atmosphere and could also be an important source of HONO in the atmosphere.

1 Introduction

It has been estimated that 1000–3000 Tg of mineral aerosols are emitted into the atmosphere annually (Jonas et al., 1995). The main components of mineral dust include

ACPD

9, 7115–7154, 2009

quartz, feldspar, carbonate (e.g. calcite, dolomite) and clay. Each of these components provides surfaces and reactants for heterogeneous reactions in the atmosphere. Many gas phase species in the atmosphere could also condense or adsorb onto mineral dust during long-range transport to impact atmospheric chemistry and climate change (Chen, 1985; Quan, 1993; Carmichael et al., 1996; Zhang et al., 2000). Modeling studies suggested that approximately 40% of nitrate formation is associated with mineral aerosols (Dentener et al., 1996). Aerosol samples taken in East Asia showed a good correlation between nitrate and calcium (Zhuang et al., 1999; Song and Carmichael, 2001; Sullivan et al., 2007).

In fresh Asian mineral aerosols, calcium is found primarily in the form of calcium carbonate ($CaCO_3$) (Song et al., 2005; Okada et al., 2005). The observed association of nitrate with calcium in mineral dust samples after long range transport suggests that after exposure to nitrogen oxides in polluted region, calcium carbonate in mineral dust had been converted to calcium nitrate, which in turn can change the composition and morphology of calcium-containing aerosols and enhance their hygroscopicity and the rates of heterogeneous reactions, thus influence the atmospheric chemistry. Calcium nitrate can also alter the optical properties of aerosols to impact radiation, cloud formation, and global climate change.

Laboratory studies have demonstrated that nitric acid (HNO_3) can react with $CaCO_3$ to form calcium nitrate (Fenter et al., 1995; Goodman et al., 2000; Hanisch and Crowley, 2001; Krueger et al., 2003a, b). The measured uptake coefficient accounting for the BET area of the samples was determined to be $(2.5\pm1)\times10^{-4}$ for HNO_3 on $CaCO_3$ under dry condition (Goodman et al., 2000). Johnson et al. (2005) determined the initial uptake coefficient of HNO_3 on $CaCO_3$ to be $(2\pm0.4)\times10^{-3}$. The net reaction probability of HNO_3 on $CaCO_3$ particles was found to increase with increasing relative humidity, from 0.003 at RH=10% to 0.21 at 80% (Liu et al., 2008a). Vlasenko et al. (2006) reported an uptake coefficient of HNO_3 on $CaCO_3$ to be 0.11 at 33% relative humidity and a humidity dependence on Arizona Test Dust.

Compared to nitric acid, little is known about the reaction of NO_2 on $CaCO_3$. The

ACPD
9, 7115–7154, 2009

uptake coefficients of NO_2 on mineral oxide particles, such as Al_2O_3, Fe_2O_3, TiO_2, have been determined to be on the order of 10^{-7} (Underwood et al., 1999); this is consistent with the results of the reaction of NO_2 on mineral dust samples from the Cape Verde Islands (Ullerstam et al., 2003).

No literature report about the uptake coefficient of NO_2 on $CaCO_3$ has been found. Considering that the concentration of NO_2 in the atmosphere is at least an order of magnitude higher than that of HNO_3, the reaction of $CaCO_3$ particles with NO_2 may comprise an important atmospheric reaction that lead to the formation of calcium nitrate during the long range transport of mineral dust. This reaction could be even more important in East Asia, where industrial regions with high NO_2 emissions are located in the path of long range transport of Asian Dust.

To understand the importance of the heterogeneous reaction of NO_2 on mineral dust, it is important to measure the uptake coefficient of NO_2 on $CaCO_3$ particles. Similar to the reaction of HNO_3 on $CaCO_3$, the reaction of NO_2 on $CaCO_3$ may also change under the influence of surface water. Therefore, it is interesting to study the reaction mechanisms and to measure the uptake coefficient of the reaction of NO_2 on $CaCO_3$ particles under dry and wet conditions.

In this study, the reactions of NO_2 on $CaCO_3$ surfaces were investigated in situ using a diffuse reflectance infrared Fourier transform spectroscopy (DRIFTS) in combination with X-ray photoelectron spectroscopy (XPS), ion chromatography (IC), and scanning electron microscopy (SEM); initial uptake coefficients were measured and the reaction mechanisms were studied under different relative humidity (RH).

2 Experimental

The infrared (IR) spectrum of the particle surface was investigated on line with DRIFTS during the reaction. The reactor of DRIFTS is a vacuum reaction chamber (Model HVC-DR2) surrounding a Harrick Scientific diffuse reflectance accessory (Model DRA-2CS) located in the sampling compartment of a Nicolet Nexus FTIR Spectrometer equipped

ACPD
9, 7115–7154, 2009

with a mercury cadmium telluride (MCT) detector. Data from 128 scans, 4 cm^{-1} resolution, taken over about 80 s were averaged for one spectrum.

Besides online infrared spectroscopy measurements, for a number of selected experiments, the reaction products on the particle surface and extractable soluble components were also measured off line using X-ray photoelectron spectroscopy (XPS) and ion chromatography (IC), respectively. The morphological changes were observed using SEM. Further details of the instruments have been described previously (Li et al., 2006).

$CaCO_3$ (>99.999%, Alfa Aesar) powder was prepared by grinding and the size of the grinded particle was about 1–10 μm with a mean value of 5.6 μm, as measured with a laser particle sizer (MasterSizer 2000, Malvern). The specific geometric surface area of the $CaCO_3$ particles was calculated to be 0.37 $m^2\,g^{-1}$ for cubic shape particles. About 20 mg of the sample was placed in the sample holder, pressed flat using a glass slide, and stored in a desiccator as previously described (Li et al., 2006). Water vapor was produced and gases were mixed using the apparatus displayed in Fig. A1. All tubes and surfaces were made of inert glass or Teflon with the exception of the stainless steel in situ reactor. Concentrations of NO_2 entering the reactor were adjusted by mixing a NO_2 standard gas (710 ppm in N_2, Center of National Standard Material Research) with pure N_2 (>99.999%) using two mass flow controllers (FC-260, Tylan, Germany). In the reactor, the NO_2 diffused to the particle surface and reacted with $CaCO_3$. The formation of the reaction products was monitored using DRIFTS. Humidity was regulated by mixing dry nitrogen with water vapor by bubbling through two glass grits in pure water (Millipore Corporation, Billerica, MA, USA). Humidity was monitored using a temperature sensor (PT100, Vaisala, Vantaa, Finland) and a humidity sensor (HM1500, Vaisala).

The volumetric BET (Brunauer, Emmett and Teller model) surface area of particles was measured with an ASAP2010 BET apparatus (Micromeritics Co., USA). The specific surface area, A_s, was determined to be 4.91 $m^2\,g^{-1}$, this is 13.3 times the specific geometric surface area of cubic shape $CaCO_3$ particles with a size of 5.6 μm.

ACPD
9, 7115–7154, 2009

After the reactions, the absolute numbers of nitrate and nitrite ions formed during the reaction were determined with IC. The reacted $CaCO_3$ particles were sonicated in 10 mL of pure water (Millipore Corporation), and then the filtered solution was analyzed using an IC (Dionex DX-500 system), which was equipped with an Ionpac AS-11HC-4 mm analytical column and a conductivity detector. Details of analyzing conditions can be found in a previous paper (Li et al., 2006).

The XPS spectra were taken on an AXIS-Ultra instrument from Kratos Analytical using monochromatic Al Kα radiation (225 W, 15 mA, 15 kV) and low–energy electron flooding for charge compensation. To compensate for surface charges effects, binding energies were calibrated using C1s hydrocarbon peak at 284.80 eV. The data were converted into VAMAS file format and imported into CasaXPS software package for manipulation and curve-fitting.

3 Results

3.1 The influence of water vapor

Calcite is the main form of $CaCO_3$ in the environment and its (104) crystal plane has the lowest energy state (de Leeuw and Parker, 1998). Both laboratory and computer modeling studies have demonstrated that at certain relative humidity, a hydrated layer on $CaCO_3$ could be dissociated by oxygen vacancy to form stable –OH that remained surface-bound even in a high vacuum (Stipp et al., 1996; McCoy and LaFemina, 1997; de Leeuw and Parker, 1998). The results of Kuriyavar et al. (2000) and Stipp (1999) demonstrated that the dissociation of water could produce surface hydroxyl on $CaCO_3$ surfaces. Species including H^+, OH^-, HCO_3^-, $Ca(OH)^+$, and $Ca(HCO_3)^+$ can exist on the surfaces of calcite and alter its surface properties (Thompson and Pownall, 1989). XPS analysis of the $CaCO_3$ particle sample showed two peaks of O1s at 531.3 eV and 533.1 eV (Fig. A2), corresponding to the oxygen atoms of $CaCO_3$ and –Ca(OH) (Stipp, 1999). The oxygen atoms of –Ca(OH) accounted for 3.4–3.6% of the total number of

ACPD
9, 7115–7154, 2009

atoms. The presence of –Ca(OH) implied that water can have a major effect on the $CaCO_3$ surface properties. Therefore, understanding water adsorption on surfaces of $CaCO_3$ particles is very important.

From the FTIR spectra of the $CaCO_3$ particle samples, we integrated the area of the stretching vibration of –OH from 3644 to 2983 cm^{-1} and plotted it as a function of RH at 296 K (Fig. 1, left axis); it demonstrated that the proportion of surface bound water increased with RH. The experimental data were fitted using the three-parameter equation of BET adsorption to determine the equivalent number of molecular layers of water, and we concluded that a monolayer of water formed on the $CaCO_3$ surface at 52% RH (Fig. 1, right axis). This suggests that the mechanisms of the heterogeneous reactions on the surface $CaCO_3$ particles could be different when RH is lower or higher than 52%.

The NO_3^- production rate on the $CaCO_3$ particle samples can be expressed as:

$$d\{NO_3^-\}/dt = k\{CaCO_3\}^m[H_2O]^q[NO_2]^n \quad (1)$$

where {x} denotes the concentration of surface species (e.g. nitrate ions and active site on $CaCO_3$), [x] denotes the concentration of species in gas phase, and m, n, and q are the reaction order for $CaCO_3$, NO_2 and H_2O, respectively. At the initial stage of the reaction, the number of NO_3^- ions formed on the surface of $CaCO_3$ is small compared to the surface active site, $\{CaCO_3\}$, which can be considered constant. At a constant NO_2 concentration, the production rate of NO_3^- is only a function of $[H_2O]$. The slope of double-log line of the NO_3^- production rate versus the water concentration should give the reaction order with respect to H_2O, q.

At a constant NO_2 concentration of 6.88×10^{15} molecules cm^{-3}, the double-log curve of the NO_3^- production rate versus the water concentration is shown in Fig. 2. The reaction order of H_2O(g) was −0.44 when RH<50%, and 0.20 when RH>50%. This indicates that at low RH, H_2O(g) inhibits the formation of surface nitrate but at high RH it had very little influence on the formation of surface nitrate. This result is consistent with the observation that at low RH, the formation of the active site on the surface of the

ACPD
9, 7115–7154, 2009

$CaCO_3$, e.g. –OH, involved the adsorbed water and the existence of adsorbed water can alter the reactivity of the particle surface (Elam et al. 1998; Hass et al., 1998; Eng et al., 2000; Hass et al., 2000). Meanwhile, water could easily adsorb onto the surface –OH, and compete with the adsorption of NO_2 (Stumm, 1992). At RH>52%, water layer forms on the surface of $CaCO_3$ and changes the reaction on the calcite surface from gas-solid to gas-liquid reaction. Thus, the water vapor plays an important role in the heterogeneous reactions of NO_2 with $CaCO_3$.

3.2 Reaction under dry conditions

Experiments under dry conditions were carried out by first heating the $CaCO_3$ at 623 K for 2 h, thus eliminating nearly all of the adsorbed water. A mixture of NO_2 and N_2 without water vapor was admitted at 296 K.

Figure 3 shows typical IR spectra of $CaCO_3$ when reacted with NO_2 under dry conditions for 0 to 100 min. Nitrate was clearly observed on the $CaCO_3$ surface. The peak at 816 cm^{-1} was assigned to the out-of-plane bending of nitrate ν_2. The peak at 1043 cm^{-1} was assigned to the symmetric stretching of nitrate ν_1 and the peak at 748 cm^{-1} was assigned to the in-plane bending of nitrate ν_4. Peaks at 1295, 1330, and 1350 cm^{-1} were assigned to the asymmetric stretching of nitrate ν_3. The ν_3 mode of nitrate on the $CaCO_3$ surface has many peaks; this is different from the nitrate ions in $Ca(NO_3)_2$ that were attributable to the adsorbed nitrate of different coordination (monodentate, bidentate, and bridging), while the nitrate ions did not form on the $CaCO_3$ surface (Borensen et al., 2000).

The asymmetric stretching of adsorbed nitric acid has been reported to be at 1710/1680 cm^{-1} (Nakamoto, 1997; Finlayson-Pitts et al., 2003). In our study, to confirm the vibration frequency of the adsorbed HNO_3, calcium sulfate ($CaSO_4$) particles were exposed to gas phase HNO_3. The IR absorption peaks of adsorbed HNO_3 were observed at 1670, and 1720 cm^{-1}; therefore, we can assign the peaks at 1670 and 1703 cm^{-1} to adsorbed HNO_3, this suggests that HNO_3 was formed when NO_2 re-

ACPD
9, 7115–7154, 2009

acted with $CaCO_3$.

The peaks at 1630 and 3520 cm^{-1} were assigned to the bending and asymmetric stretching of crystal hydrate water. Compared with the vibration frequencies of the crystallized water in $Ca(NO_3)_2{\cdot}4H_2O$ at 1640 cm^{-1} and 3490 cm^{-1}, a shift of both peaks occurred, due to the decreased hydrogen bonding. The asymmetric stretching shifted to the higher wave number, and the bending shifted to the lower wave number. The peaks at 3140 and 3330 cm^{-1} were assigned to surface adsorbed water, both peaks decreased as the reaction proceeded until the peaks for crystal hydrate water at 1630 cm^{-1} and 3520 cm^{-1} appeared.

The XPS spectrum of $CaCO_3$ particle that reacted with 1.06×10^{15} molecules cm^{-3} NO_2 for 626 min (Fig. A3a) showed the peak of nitrogen of +5 valence at 407.3 eV, and confirmed the formation of nitrate. The formation of nitrate was further confirmed by IC analysis of reacted $CaCO_3$ particles (Fig. A3b). However, no nitrite was detected with both XPS and IC, this is probably due to the reason that HONO formed in the reaction was released into the gas phase and carried away by N_2.

Figure 4 shows the formation of nitrate on $CaCO_3$ through the reaction of NO_2 as a function of time. The amount of nitrate formed is represented by the integrate absorbance (I_A) of the IR peak area between 1077 and 1013 cm^{-1}. As the reaction proceeded, the nitrate concentration on the calcite surface increased and the rate of nitrate formation increased with higher NO_2 concentrations. The nitrate formation process could be divided into three stages: stage I lasted from the initiation of the reaction until I_A reached 0.3, stage II was the transition stage when the increase of I_A was slowing down between 0.3 and 0.4, and stage III was the growth stage when I_A>0.4 and the increase rate of I_A reached to a constant.

The amount of nitrate ions formed on the particles $\{NO_3^-\}$ was determined with a linear relationship between I_A in the range of 1073–1013 cm^{-1} and the amount of nitrate determined by ion chromatography $\{NO_3^-\}$:

$$\{NO_3^-\} = f \times I_A \quad (2)$$

ACPD
9, 7115–7154, 2009

The conversion factor f was found to be independent of reaction time and NO_2 concentration as long as the experiment was completed at a stage when the absorption of the nitrate band was still growing. For our study, f was calculated to be 1.89×10^8 molecules/I_A.

Using f, the production rate of nitrate $d\{NO_3^-\}/dt$ was calculated, and the reaction order of NO_2 on $CaCO_3$ particles was obtained from the slope of the double-log plots of $d\{NO_3^-\}/dt$ versus NO_2 concentrations (Fig. 5). In stage I the reaction order of NO_2 was 1.63±0.23 and in stage II 0.41±0.55. This means that the nitrate formation with respect to NO_2 was a second-order reaction in the initial stage (I) and a zero-order reaction in the transition stage (II).

3.3 Reaction under wet conditions

Experiments of $CaCO_3$ reaction with NO_2 under wet conditions were carried out using non-heat-treated $CaCO_3$ particles at 296 K with RH=60–71%. Figure 6 shows the typical IR spectra of $CaCO_3$ when NO_2 entered the reactor under wet conditions, at reaction times from 0 to 60 min.

The peak at 1048 cm^{-1} was assigned to the symmetric stretching ν_1 of nitrate, the peak at 1344 cm^{-1} to the asymmetric stretching ν_3 of nitrate. The peak at 1251 cm^{-1} was assigned to the asymmetric stretching ν_3 of nitrite. The peak at 1688 cm^{-1} was assigned to the adsorption peak of HNO_3 and the peak at 1636 cm^{-1} to the bending of the surface adsorbed water; the peak at 1472 cm^{-1} appeared in the range of peaks for the asymmetric stretching of carbonate and was assigned to the carbonate vibration peak. Compared to the corresponding peak observed under dry conditions, these peaks had all shifted more or less. We attributed these shifts to the changed environment caused by increased surface adsorbed water under wet conditions.

The peaks at 1525 and 1540 cm^{-1} were in the range of asymmetric stretching of bicarbonate and were assigned to the bicarbonate vibration peaks (Al-Hosney and Grassian 2004; Al-Abadleh et al., 2005). Negative peaks at 1472, 1525, and 1540 cm^{-1}

ACPD
9, 7115–7154, 2009

were similar to the negative peaks from the reaction of HNO_3 with $CaCO_3$ (Fig. A5). This indicated that the intermediate products HCO_3^- and H_2CO_3 were formed during the reaction of NO_2 with $CaCO_3$. The result is consistent with the findings of Al-Hosney and Grassian (2004) that H_2CO_3 was the intermediate product when HNO_3, SO_2, HCOOH and CH_3COOH reacted with $CaCO_3$.

The formation of nitrate and nitrite was further confirmed by the XPS spectrum of $CaCO_3$ particles reacting with 1.06×10^{15} molecules cm^{-3} of NO_2 for 30 min at RH=80±2%, which demonstrated the existence of N of +5 valence and +3 valence as shown in Fig. A4a, and the formation of nitrate and nitrite was shown in IC chromatogram of Fig. A4b.

To obtain the change rate of each peak, Gaussian peak-fitting was used within the spectral range of 1750–1150 cm^{-1} (Fig. 7a). Figure 7b shows the integrate absorbance of nitrate peak at 1344 cm^{-1} increased during the reaction while that of the carbonate peaks at 1472, 1525, and 1540 cm^{-1} decreased with time, indicating that nitrate was produced when $CaCO_3$ was consumed.

The nitrite ion peak at 1251 cm^{-1} and HNO_3 peak at 1688 cm^{-1} increased initially and subsequently decreased, implying that the decrease of nitrite was related to the decrease of HNO_3. It was inferred that the increase of adsorbed nitric acid caused the release of nitrite in the form of gaseous HONO which led to the decreased of both nitrite ion and nitric acid. The adsorbed water peak at 1636 cm^{-1} exhibited a linear increase initially but later reached a plateau, demonstrating that the $CaCO_3$ particle surface was gradually saturated with adsorbed water.

Figure 8 shows the nitrate formation as a function of time during the reaction of $CaCO_3$ with NO_2 under wet (RH=60–71%) conditions. The integrated absorbance was in the range of 1077–1013 cm^{-1}. Unlike the reaction under dry conditions, under wet conditions, the nitrate on the $CaCO_3$ surface increased linearly with time but did not become saturated during the experimental period, and the nitrate formation rate increased with the increasing of NO_2 concentrations.

Using the conversion factor $f=1.89\times10^8$ molecules/I_A, the integrate absorbance of

the nitrate peak in the range of 1077–1013 cm^{-1} was converted to the number of nitrate ions formed on $CaCO_3$ particle surface $\{NO_3^-\}$. The reaction order of NO_2 was obtained from the slope of the double-log plot of the nitrate production rate $d\{NO_3^-\}/dt$ versus the NO_2 concentration (Fig. 9). The slope of the curve was 0.94±0.10; this means that under wet conditions, the NO_2 reaction on $CaCO_3$ particles is first order with respect to NO_2.

3.4 Uptake coefficient

Reactive uptake coefficient or reaction probability, γ, is defined as the ratio of reactive gas-surface collision rate to the total gas-surface collision rate. The reactive uptake coefficient of NO_2 by the surface of the $CaCO_3$ particles is

$$\gamma = \frac{dN(NO_2)/dt}{Z} \tag{3}$$

$$Z = \tfrac{1}{4} A \omega n \tag{4}$$

where $N(NO_2)$ is the number of reactive NO_2 collisions with the surface, Z is the total gas-surface collision rate of NO_2 on the surface of $CaCO_3$, A is the surface area of $CaCO_3$ particles (BET surface area was used here), ω is the mean speed of the gas molecule, and n is the concentration of gas phase species. The rate of reactive collisions can be obtained from the production rate of nitrate $d\{NO3-\}/dt$, the reactive uptake coefficient then become:

$$\gamma = \frac{2d\left\{NO_3^-\right\}/dt}{Z} \tag{5}$$

Previous studies show that the reaction of NO_2 with particles was through N_2O_4 (Finlayson-Pitts et al., 2003), then the reactive NO_2 loss rate in the gas phase is twice of the nitrate formation rate.

ACPD
9, 7115–7154, 2009

The nitrate formation rate $d\{NO_3^-\}/dt$ could be calculated from the curve of nitrate formation as a function of time, and the nitrate formation rate in the initial stage of the reaction was used for calculating the initial uptake coefficient γ_0. Table 1 lists the initial uptake coefficient of NO_2 on $CaCO_3$ particles under both dry and wet (RH=60–71%) conditions. The initial uptake coefficient under dry conditions was $(1.09\pm0.25)\times10^{-7}$, while under wet conditions, it was slightly lower, with a value of $(0.63\pm0.33)\times10^{-7}$. To further investigate the influence of RH on the uptake of NO_2 on $CaCO_3$ particle, the initial uptake coefficient of the reaction was determined as a function of RH. Figure 10 shows the results. As RH increased, γ_0 decreased initially with increasing RH; at RH=45–53%, γ_0 showed a turning point and jumped to a higher value at RH=53%; with RH>53%, γ_0 started to increase slightly with the increasing RH.

The change of γ_0 with RH demonstrates the influence of water vapor on the reaction mechanism of NO_2 on $CaCO_3$ particles. When RH<53%, H_2O was competing with NO_2 molecules for reactive sites on the surface of $CaCO_3$ particles, the initial uptake coefficient of NO_2 was therefore decreasing with increasing RH.

As described in the above section, at RH=52±2%, a monolayer of adsorbed water was formed on the surface of the $CaCO_3$ particles, hence with RH>52%, the reaction of NO_2 on $CaCO_3$ particles was controlled by the reaction of NO_2 with surface condensed water on the $CaCO_3$ particles. This may explain why the increase of RH had little influence on γ_0 when RH was larger than 52%. The formation of a water layer on $CaCO_3$ particles suggests that the reaction mechanism of NO_2 on $CaCO_3$ became different from that when RH was lower than 52%.

It is puzzling to see from both Table 1 and Fig. 10 that under dry and wet conditions, γ_0 were varied within a narrow range of 0.6×10^{-7}–1.2×10^{-7}. Mertes and Wahner (1995) have measured a lower limit of the mass accommodation coefficient of NO_2 on aqueous surfaces of $\alpha\geq2\times10^{-4}$ at 278 K surface temperature. This suggests that at RH>52%, with the formation of water layer on the surface of $CaCO_3$ particles, γ_0 of NO_2 on $CaCO_3$ particles should have a value much higher than 10^{-7}. The possible reason for a lower γ_0 value is that we used the specific BET surface area of $CaCO_3$

particles (4.91 $m^2 g^{-1}$) to calculate γ_0, while at RH>52%, the water layer formed could make the surface of $CaCO_3$ particles smoother with less pores, and the available surface area for the reaction should be close to the geometric surface area of a cubic shape particle. Using 0.37 $m^2 g^{-1}$ as the specific geometric surface area of $CaCO_3$ particle samples, from Table 1 we calculated γ_0 at RH=60–71% to be (0.84±0.44) $\times 10^{-6}$; this should be the upper limit of γ_0 and is about ten times higher than γ_0 at RH<52%, when BET surface area was used. The uptake coefficient for HNO_3 on $CaCO_3$ was determined to be at a level of 10^{-4} (e.g. Goodmann et al., 2000). Considering that NO_2 concentrations in the atmosphere is orders of magnitude higher than that of HNO_3, at RH>52%, NO_2 may have similar importance of HNO_3 in the heterogeneous reactions with $CaCO_3$ particle in the atmosphere.

4 Discussion

We concluded from the above results that water vapor had a major influence on the heterogeneous reaction mechanism of NO_2 with $CaCO_3$. The reaction mechanism was different before and after a monolayer of water was formed. Prior to the formation of the monolayer of water on $CaCO_3$ surface, –OH was produced on the calcite surface via the dissociation of water by oxygen vacancy and this seems to be the rate determining factor for the reaction. After formation of a monolayer of water, surface condensed water participated in the reaction. We discuss the reaction mechanisms for both of these two conditions below.

4.1 Mechanism under dry conditions

Under dry conditions, the reaction mechanism proceeded as shown in Fig. 11a. At low RH, there was still some water vapor remaining and the surface adsorbed water on the

ACPD
9, 7115–7154, 2009

$CaCO_3$ surface equilibrated with water vapor, as shown in Reaction (R1):

$$H_2O(g) \underset{k_{-1}}{\overset{k_1}{\rightleftharpoons}} H_2O(a) \quad \text{(R1)}$$

Surface-adsorbed water existed on the $CaCO_3$ surface despite heating at 623 K for 2 h. The adsorbed water on the $CaCO_3$ surface was dissociated by an oxygen vacancy site (O) to form the active site S·(OH)H that was stable even at high temperature and high vacuum. When the surface-adsorbed water increased, the surface active site converted to adsorbed-water due to the action of the hydrogen bond:

$$\text{site (O)} + 2H_2O(a) \underset{k_{-2}}{\overset{k_2}{\rightleftharpoons}} S \cdot (OH)H + H_2O(a) \quad \text{(R2)}$$

Finlayson-Pitts et al. (2003) found NO_2 was likely to form nitrogen dioxide dimmers (nitrogen tetraoxide, N_2O_4) at high concentrations, then N_2O_4 was adsorbed to the particle surface.

$$2NO_2(g) \underset{k_{-3}}{\overset{k_3}{\rightleftharpoons}} N_2O_4(g) \quad \text{(R3)}$$

$$N_2O_4(g) \underset{k_{-4}}{\overset{k_4}{\rightleftharpoons}} N_2O_4(a) \quad \text{(R4)}$$

N_2O_4 reacted with the surface active site forming adsorbed nitric acid HNO_3 and nitrous acid HONO, as illustrated in Reaction (R5):

$$N_2O_4(a) + S \cdot (OH)H \xrightarrow{k_5} HNO_3(a) + HONO(g) \quad \text{(R5)}$$

Previous studies showed that HONO was unlikely to adsorb onto the calcite surface, but rather being released into the gas phase. Although we could not detect gas phase HONO, we did detect adsorbed HNO_3 with DRIFTS.

ACPD
9, 7115–7154, 2009

Surface adsorbed water was in equilibrium with water vapor, see Eq. (6), where [x] indicates the concentration of gas phase species and {x} denotes the concentration of surface adsorbed species and active sites.

$$\{H_2O\} = \frac{k_1}{k_{-1}}[H_2O] = K_1[H_2O] \quad (6)$$

At the initial stage, surface-adsorbed water increased with RH, and the surface active site S·(OH)H was converted to adsorbed water.

$$\{S\cdot(OH)H\} = \frac{k_2}{k_{-2}}\{site(O)\}\{H_2O\} = K_2\{site(O)\}\{H_2O\} \quad (7)$$

NO_2 was in equilibrium with N_2O_4 in the gas phase,

$$[N_2O_4] = \frac{k_3}{k_{-3}}[NO_2]^2 = K_3[NO_2]^2 \quad (8)$$

No adsorbed N_2O_4 was observed on the particle surface, suggesting N_2O_4 could be treated as an intermediate in the reaction:

$$\frac{d\{N_2O_4\}}{dt} = k_4[N_2O_4] - k_{-4}\{N_2O_4\} - k_5\{N_2O_4\}\{S\cdot(OH)H\} = 0 \quad (9)$$

Assuming the HNO_3 formed was quickly converted to NO_3^- on the surface of $CaCO_3$, Then

$$\frac{d\{NO_3^-\}}{dt} = \frac{d\{HNO_3\}}{dt} = k_5\{N_2O_4\}\{S\cdot(OH)H\} \quad (10)$$

Combining Eqs. (6, 7, 8, 9, and 10), one can get

$$\frac{d\{NO_3^-\}}{dt} = \frac{K_1K_2K_3k_4k_5[NO_2]^2\{site(O)\}[H_2O]}{k_{-4}+K_1K_2k_5\{site(O)\}[H_2O]} \quad (11)$$

Equation (11) shows that, at the initial stage of the reaction, the amount of surface active site was relative large and formation of HNO_3 on the $CaCO_3$ surface was a second-order reaction with respect to NO_2; this is consistent with the measured reaction order of 1.63±0.23 obtained from Fig. 5.

4.2 Mechanism under wet conditions

In the above section, we showed that at RH>52%, water condensed on $CaCO_3$ forming a monolayer of adsorbed water. Here, the wet conditions refer to the conditions when RH>52%. The reaction mechanism under wet conditions was illustrated by the general scheme in Fig. 11b. NO_2 was adsorbed on $CaCO_3$ to form adsorbed NO_2(a):

$$NO_2(g) \underset{k_{-6}}{\overset{k_6}{\rightleftharpoons}} NO_2(a) \quad \text{(R6)}$$

Previous studies have demonstrated that the disproportionation reaction of NO_2 with surface adsorbed water was a first-order reaction with the adsorption of NO_2 being the rate-limiting step (Svensson et al., 1987; Jenkin et al., 1988). The nitrite and nitrate formed on the particle surface was attributed to the reaction of surface-adsorbed water with NO_2; i.e., adsorbed $NO_2(a)$ reacted with condensed water $H_2O(a)$ to form adsorbed $HNO_3(a)$ and gaseous $HONO(g)$.

$$H_2O(a) + 2NO_2(a) \xrightarrow{k_7} HNO_3(a) + HONO(g) \quad \text{(R7)}$$

At the initial stage, HONO dissolved in adsorbed water to form nitrite. As the concentration of $HNO_3(a)$ increased, the surface pH decreased and nitrite was escaped from the surface as gaseous HONO. Meanwhile, $HNO_3(a)$ reacted with $CaCO_3$ to form H_2CO_3 and $Ca(NO_3)_2$.

$$2HNO_3(a) + CaCO_3(s) \xrightarrow{k_8} Ca(NO_3)_2(s) + H_2CO_3(a) \quad \text{(R8)}$$

ACPD
9, 7115–7154, 2009

Afterward, H_2CO_3 decomposed in adsorbed water to form H_2O and CO_2, resulting in the decrease of HCO_3^- and CO_3^{2-} on the surface.

$$H_2CO_3(a) \longrightarrow H_2O(g) + CO_2(g) \quad \text{(R9)}$$

$Ca(NO_3)_2$ has strong hygroscopic property and the $Ca(NO_3)_2$ particles were in the form of solution droplets at RH>10% (Liu et al., 2008b); this caused the broadened peak for adsorbed water in the IR spectrum.

$$Ca(NO_3)_2(s) + nH_2O(a) \rightleftarrows Ca(NO_3)_2 \cdot nH_2O \quad \text{(R10)}$$

Since the adsorption of NO_2 was the rate-limiting step and $HNO_3(a)$ was the intermediate product, the rate of nitrate production in the presence of excess surface water could be expressed as the following.

$$\frac{d\{NO_3^-\}}{dt} = \frac{1}{2}k_6[NO_2] \quad (12)$$

Equation (12) shows the surface nitrate formation with respect to NO_2 as a first order reaction; this is consistent with the experimental result of 0.94±0.10 and results in the literature.

5 Conclusions

The initial uptake coefficient of NO_2 on $CaCO_3$ particles γ_0 was found to change with increasing relative humidity. Using BET surface area, γ_0 under dry conditions (RH~0%) was determined to be $(1.09\pm0.25)\times10^{-7}$, while under "wet" conditions (RH=60–71%), it was slightly lower, with a value of $(0.63\pm 0.33)\times10^{-7}$. Our results show that relative humidity had a major influence on the surface properties of $CaCO_3$ particles by not only influencing the initial uptake coefficient but also by changing the reaction mechanism. At RH<52%, surface –OH produced via the dissociation of surface-adsorbed water

ACPD
9, 7115–7154, 2009

by an oxygen vacancy on the $CaCO_3$ surface was the rate determining factor in the reaction. Before surface –OH was depleted, the reaction was second order in NO_2. At RH>52%, a water layer of more than a monolayer was formed and NO_2 reacted with water on the surface of $CaCO_3$ to produce HNO_3 and HONO; at this stage, the reaction was the first order in NO_2.

At RH>52%, the water layer formed could make the surface smoother with less pores, and the surface area should be much smaller than the BET surface area. Using $0.37\,m^2\,g^{-1}$ as the specific geometric surface area of $CaCO_3$ particle samples, we calculated γ_0 at RH=60–71% to be $(0.84\pm0.44)\times10^{-6}$; this is about ten times higher than that under dry conditions and could be used as the upper limit of γ_0. Considering the uptake coefficient for HNO_3 on $CaCO_3$ is at a level of 10^{-4} and NO_2 concentrations in the atmosphere is orders of magnitude higher than that of HNO_3, at RH>52 %, NO_2 should have similar importance of HNO_3 in the heterogeneous reactions with $CaCO_3$ particle in the atmosphere, and the NO_2 reaction with water adsorbed on $CaCO_3$ could also be an important source of HONO in the atmosphere. Further efforts to detect HONO formed in the reaction of NO_2 on $CaCO_3$ particles are under way.

Acknowledgements. This work was supported by the National Basic Research Priorities Program (Grant No. 2002CB410802) and National Natural Science Foundation of China (Grant No. 40490265).

References

Al-Abadleh, H. A., Al-Hosney, H. A., and Grassian, V. H.: Oxide and carbonate surfaces as environmental interfaces: the importance of water in surface composition and surface reactivity, J. Mol. Catal. A – Chem., 228, 47–54, 2005.

Al-Hosney, H. A. and Grassian V. H.: Carbonic acid: An important intermediate in the surface chemistry of calcium carbonate, J. Am. Chem. Soc., 126, 8068–8069, 2004.

Boerensen, C., Kirchner, U., Scheer, V., Vogt, R., and Zellner, R.: Mechanism and kinetics of the reactions of NO_2 or HNO_3 with alumina as a mineral dust model compound, J. Phys. Chem. A, 104, 5036–5045, 2000.

Carmichael , G. R., Zhang ,Y., Chen, L. L., Hong, M. S., and Ueda, H.: Seasonal variation of aerosol composition at Cheju Island, Korea, Atmos. Environ., 30, 2407–2416, 1996.
Chen, L. Q.: Long range atmospheric transport of China desert aerosol to north Pacific Ocean, Acta Oceanol. Sin., 7, 554–560, 1985 (in Chinese).
de Leeuw, N. H. and Parker, S. C.: Surface structure and morphology of calcium carbonate polymorphs calcite, aragonite, and vaterite: an atomistic approach, J. Phys. Chem. B, 102, 2914–2922, 1998.
Dentener, F. J., Carmichael, G. R., Zhang, Y., Lelieveld, J., and Crutzen, P. J.: Role of mineral aerosol as a reactive surface in the global troposphere, J. Geophys. Res. Atmos., 101, 22869–22889, 1996.
Elam, J. W., Nelson, C. E., Cameron, M. A., Tolbert M. A., and George, S. M.: Adsorption of H_2O on a single-crystal alpha-Al_2O_3(0001) surface, J. Phys. Chem. B, 102, 7008–7015, 1998.
Eng, P. J., Trainor, T. P., Brown, Jr., G. E., Waychunas, G. A., Newville, M., Sutton, S. R., and Rivers, M. L.: Structure of the hydrated alpha-Al_2O_3 (0001) surface, Science, 288, 1029–1033, 2000.
Fenter, F. F., Caloz, F., and Rossi, M. J.: Experimental-Evidence for the Efficient Dry Deposition of Nitric-Acid on Calcite, Atmos. Environ., 29, 3365–3372, 1995.
Finlayson-Pitts, B. J., Wingen, L. M., Sumner, A. L., Syomin, D., and Ramazan, K. A.: The heterogeneous hydrolysis of NO_2 in laboratory systems and in outdoor and indoor atmospheres: An integrated mechanism, Phys. Chem. Chem. Phys., 5, 223–242, 2003.
Goodman, A. L., Underwood, G. M., and Grassian, V. H.: Heterogeneous Reaction of NO_2: Characterization of Gas-Phase and Adsorbed Products from the Reaction, $2NO_2(g)+H_2O(a)$ f $HONO(g)+HNO_3(a)$ on Hydrated Silica Particles, J. Phys. Chem. A, 103, 7217–7223, 1999.
Goodman, A. L., Underwood, G. M., and Grassian, V. H.: A laboratory study of the heterogeneous reaction of nitric acid on calcium carbonate particles, J. Geophys. Res. Atmos., 105, 29053–29064, 2000.
Hanisch, F. and Crowley, J. N.: Heterogeneous reactivity of gaseous nitric acid on Al_2O_3, $CaCO_3$, and atmospheric dust samples: A Knudsen cell study, J. Phys. Chem. A, 105, 3096–3106, 2001.
Hass, K. C., Schneider, W. F., Curioni, A., and Andreoni, W.: The chemistry of water on alumina surfaces: Reaction dynamics from first principles, Science, 282, 265–268, 1998.
Hass, K. C., Schneider, W. F., Curioni A., and Andreoni, W.: First-principles molecular dynamics

simulations of H_2O on alpha-Al2O3 (0001), J. Phys. Chem. B, 104, 5527–5540, 2000.
Jenkin, M. E., Cox, R. A., and Williams D. J.: Laboratory Studies of the kinetics of formation of nitrous-acid from the thermal-reaction of nitrogen-dioxide and water-vapor, Atmos. Environ., 22, 487–498, 1988.
Johnson, E. R., Sciegienka, J., Carlos-Cuellar, S., and Grassian, V. H.: Heterogeneous Uptake of Gaseous Nitric Acid on Dolomite ($CaMg(CO_3)_2$) and Calcite ($CaCO_3$) Particles: A Knudsen Cell Study Using Multiple, Single, and Fractional Particle Layers, J. Phys. Chem. A, 109, 6901–6911, 2005.
Jonas, P. R., Charlson, R. J., Rodhe, H., Anderson, T. L., Andreae, M. O., Dutton, E., Graf, H., Fouquart, Y., Grassl, H., Heintzenberg, J., Hobbs, P. V., Hofmann, D., Hubert, B., et al.: Aerosols, in: Climate Change 1994: Radiative Forcing of Climate Change, edited by: Houghton, J. T., Meira Filho, L. G., Bruce, J., Lee, H., Callander, B. A., Haites, E., Harris, N., and Maskell, K., Cambridge University Press, Cambridge, UK, 127–162, 1995.
Krueger, B. J., Grassian, V. H., Iedema, M. J., Cowin, J. P., and Laskin, A.: Probing heterogeneous chemistry of individual atmospheric particles using scanning electron microscopy and energy-dispersive X-ray analysis, Anal. Chem., 75, 5170–5179, 2003a.
Krueger, B. J., Grassian, V. H., Laskin, A., and Cowin, J. P.: The transformation of solid atmospheric particles into liquid droplets through heterogeneous chemistry: Laboratory insights into the processing of calcium containing mineral dust aerosol in the troposphere, Geophys. Res. Lett., 30, 1148, doi:10.1029/2002GL016563, 2003b.
Kuriyavar, S. I., Vetrivel, R., Hegde, S. G., Ramaswamy, A. V., Chakrabarty, D., and Mahapatra, S.: Insights into the formation of hydroxyl ions in calcium carbonate: temperature dependent FTIR and molecular modelling studies, J. Mater. Chem., 10, 1835–1840, 2000.
Li, H. J., Zhu, T., Ding, J., Chen, Q., and Xu, B. Y.: Heterogeneous reaction of NO_2 on the surface of NaCl particles, Sci. China, Ser. B Chem., 49, 371–378, 2006.
Liu, Y., Gibson, E. R., Cain, J. P., Wang, H., Grassian, V. H., and Laskin, A.: Kinetics of Heterogeneous Reaction of $CaCO_3$ Particles with Gaseous HNO_3 over a Wide Range of Humidity, J. Phys. Chem. A, 112, 1561–1571, 2008a.
Liu, Y. J., Zhu, T., Zhao, D. F., and Zhang, Z. F.: Investigation of the hygroscopic properties of $Ca(NO_3)_2$ and internally mixed $Ca(NO_3)_2/CaCO_3$ particles by micro-Raman spectrometry, Atmos. Chem. Phys., 8, 7205–7215, 2008b, http://www.atmos-chem-phys.net/8/7205/2008/.
McCoy, J. M. and LaFemina, J. P.: Kinetic Monte Carlo investigation of pit formation at the $CaCO_3$(10(1)over-bar4) surface-water interface, Surf. Sci., 373, 288–299, 1997.

Mertes, S. and Wahner, A.: Uptake of Nitrogen Dioxide and Nitrous Acid on Aqueous Surfaces, J. Phys. Chem., 99, 14000–14006, 1995.
Nakamoto, K.: Infrared and Raman Spectra of Inorganic and Coordination Compounds Part A, New York, John Wiley & Sons, 221–247, 1997.
Okada, K., Qin, Y., and Kai, K.: Elemental composition and mixing properties of atmospheric mineral particles collected in Hohhot, China, Atmos. Res., 73, 45–67, 2005.
Quan, H.: Discussion of the transport route of dust storm and loess aerosol from Northwest China at the high altitude, Environ. Sci., 14, 60–65, 1993 (in Chinese).
Song, C. H. and Carmichael, G. R.: Gas-particle partitioning of nitric acid modulated by alkaline aerosol, J. Atmos. Chem., 40, 1–22, 2001.
Song, C. H., Maxwell-Meier, K., Weber, R. J., Kapustin, V., and Clarke, A.: Dust composition and mixing state inferred from airborne composition measurements during ACE-Asia C130 Flight #6, Atmos. Environ., 39, 359–369, 2005.
Stipp, S. L. S., Gutmannsbauer, W., and Lehmann, T.: The dynamic nature of calcite surfaces in air, Am. Mineral., 81, 1–8, 1996.
Stipp, S. L. S.: Toward a conceptual model of the calcite surface: Hydration, hydrolysis, and surface potential, Geochim. Cosmochim. Acta, 63, 3121–3131, 1999.
Stumm, W.: Chemistry of the solid-water interface: processes at the mineral-water and particle-water interface in natural systems, New York, John Wiley & Sons, 168 pp., 1992.
Sullivan, R. C., Guazzotti, S. A., Sodeman, D. A., and Prather, K. A.: Direct observations of the atmospheric processing of Asian mineral dust, Atmos. Chem. Phys., 7, 1213–1236, 2007, http://www.atmos-chem-phys.net/7/1213/2007/.
Svensson, R., Ljungstrom, E., and Lindqvist, O.: Kinetics of the Reaction between Nitrogen Dioxide and Water Vapor, Atmos. Environ., 21, 1529–1539, 1987.
Thompson, D. W. and Pownall, P. G.: Surface Electrical-Properties of Calcite, J. Colloid Interface Sci., 131, 74–82, 1989.
Ullerstam, M., Johnson, M. S., Vogt, R., and Ljungström, E.: DRIFTS and Knudsen cell study of the heterogeneous reactivity of SO_2 and NO_2 on mineral dust, Atmos. Chem. Phys., 3, 2043–2051, 2003, http://www.atmos-chem-phys.net/3/2043/2003/.
Underwood, G. M., Miller, T. M., and Grassian, V. H.: Transmission FT-IR and Knudsen Cell Study of the Heterogeneous Reactivity of Gaseous Nitrogen Dioxide on Mineral Oxide Particles, J. Phys. Chem. A, 103, 6184–6190, 1999.
Vlasenko, A., Sjogren, S., Weingartner, E., Stemmler, K., Gäggeler, H. W., and Ammann, M.:

Effect of humidity on nitric acid uptake to mineral dust aerosol particles, Atmos. Chem. Phys., 6, 2147–2160, 2006, http://www.atmos-chem-phys.net/6/2147/2006/.
Zhang, D. Z., Shi, G. Y., Iwasaka, Y., and Hu, M.: Mixture of sulfate and nitrate in coastal atmosphere aerosol :individual particle studies in Qingdao (36 degrees 04′ N, 120 degrees 21′ E), China, Atmos. Environ., 34, 2669–2679, 2000.
Zhuang, H., Chan, C. K., Fang, M., and Wexler, A. S.: Formation of nitrate and non-sea-salt sulfate on coarse particles, Atmos. Environ., 33, 4223–4233, 1999.

ACPD
9, 7115–7154, 2009

Table 1. Initial uptake coefficient of NO_2 on $CaCO_3$ particles under dry and wet conditions. The RH was measured at 296 K.

replicate time	$[NO_2]$ (10^{15} molecule cm^{-3})	$\gamma_0 \pm 2\sigma$ (10^{-7})	RH (%)
14	6.90–16.84	1.09±0.25	dry
5	4.58–11.40	0.63±0.33	60–71

ACPD
9, 7115–7154, 2009

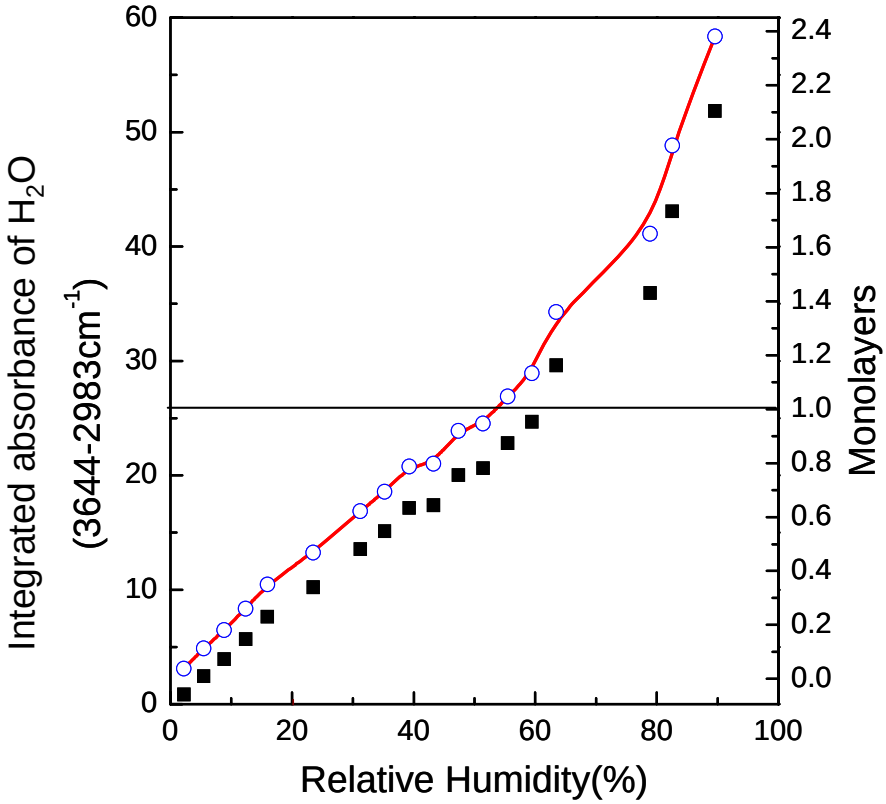

Fig. 1. Isotherm adsorption curve of water vapor on $CaCO_3$ particles at 296 K. IR absorbance of the stretching vibration of –OH of adsorbed water is integrated between 3644 and 2983 cm^{-1}. A monolayer of water was formed at 52% RH, based on the calculation using the BET equation (filled black square indicates the integration area of water; ○ denotes the number of single-molecule water layers).

ACPD
9, 7115–7154, 2009

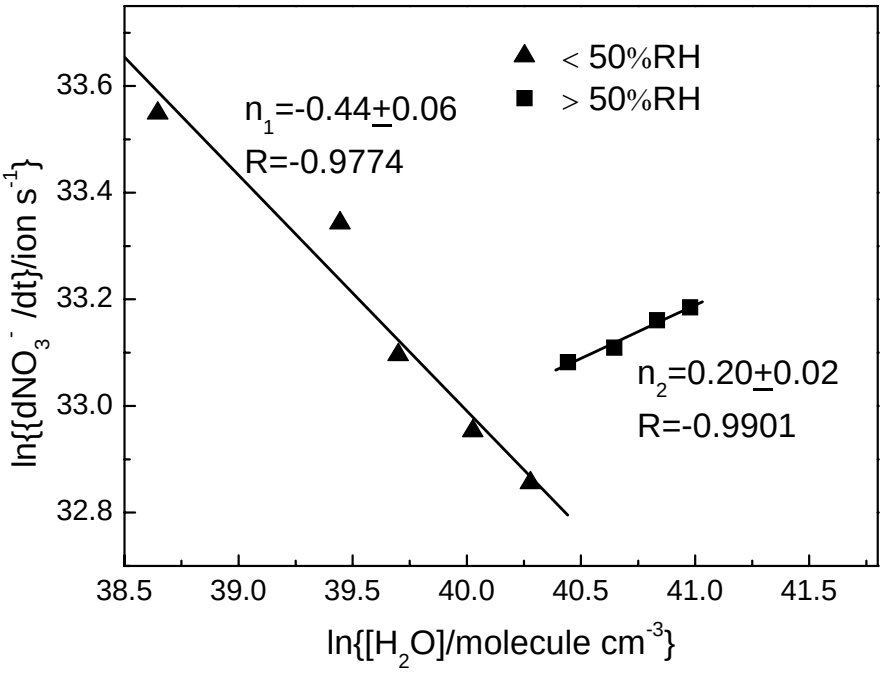

Fig. 2. Double-log curve of NO_3^- production rate versus $[H_2O]$. The reaction order with respect to $H_2O(g)$ was −0.44 at RH<50%, and was 0.20 at RH>50%.

ACPD
9, 7115–7154, 2009

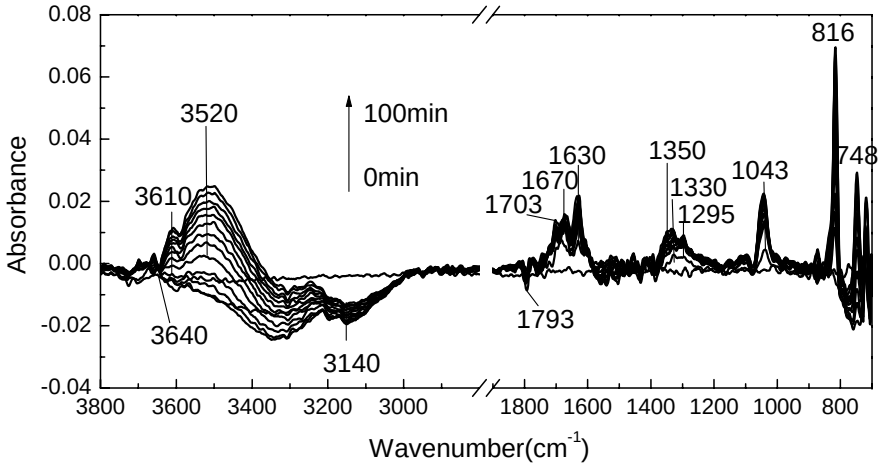

Fig. 3. Typical IR spectra of $CaCO_3$ particles after reaction with NO_2 at 296 K and reaction times of 0 to 100 min. RH was <10%, NO_2 concentration was 1.22×10^{16} molecule cm^{-3}.

ACPD
9, 7115–7154, 2009

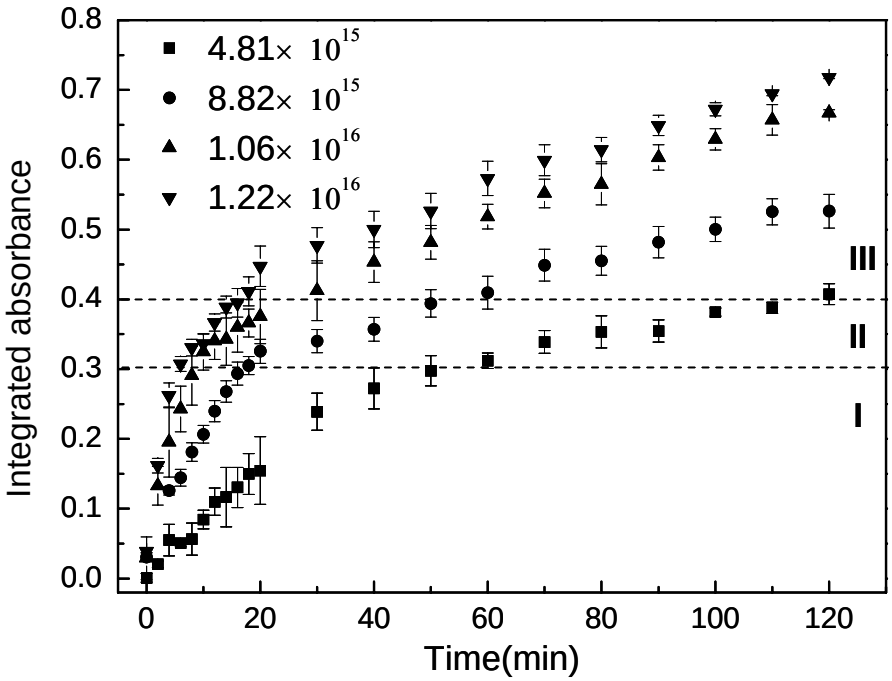

Fig. 4. Nitrate formation as a function of time during the reaction of $CaCO_3$ with NO_2. The nitrate concentration is represented by the integrated absorbance of the peak area between 1077 and 1013 cm^{-1}. The NO_2 concentration was changed from 4.81×10^{15} to 1.22×10^{16} molecule cm^{-3}. The data points and the error bars are the average value and the standard deviation of three duplicate experiments.

ACPD
9, 7115–7154, 2009

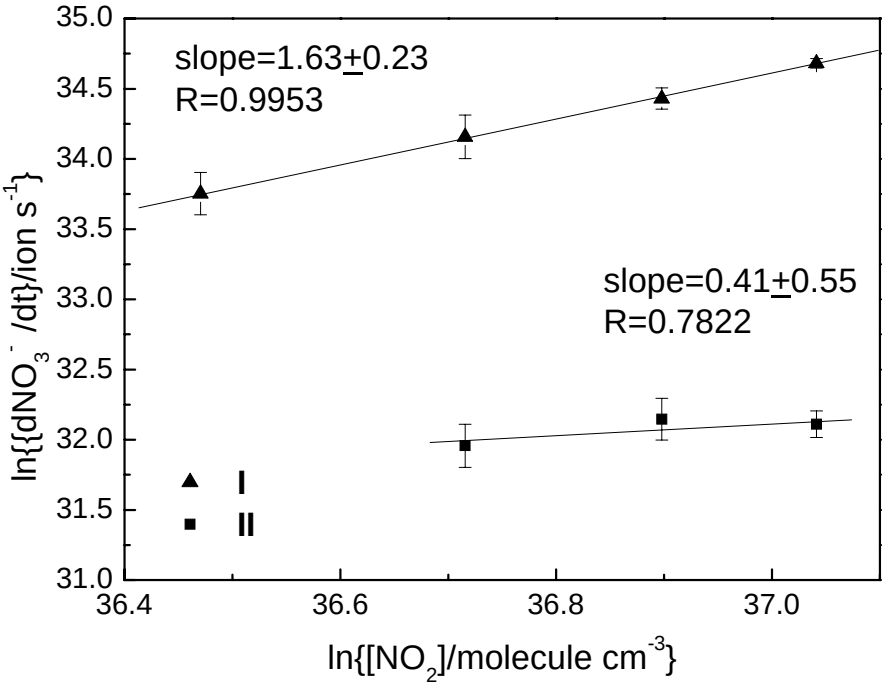

Fig. 5. Double-log curves of nitrate-producing rate versus NO_2 concentration. The data points and error bars are the average values and standard deviations of three replicate experiments. The reaction order was of NO_2 1.63±0.23 in stage I, and 0.41±0.55 in transition stage II.

ACPD
9, 7115–7154, 2009

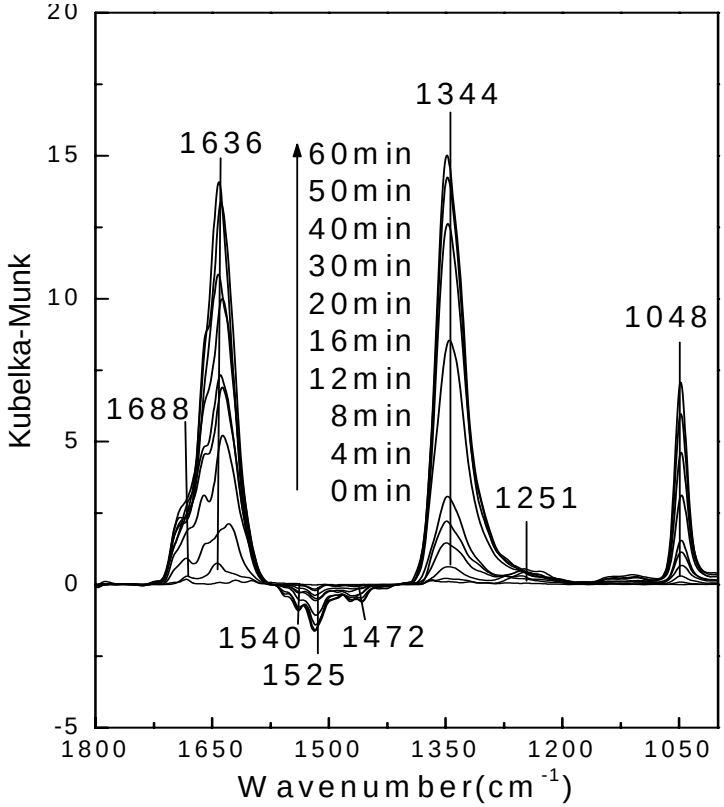

Fig. 6. Typical IR spectrum for $CaCO_3$ reacted with NO_2 under wet condition at reaction time of 0 to 60 min.

ACPD
9, 7115–7154, 2009

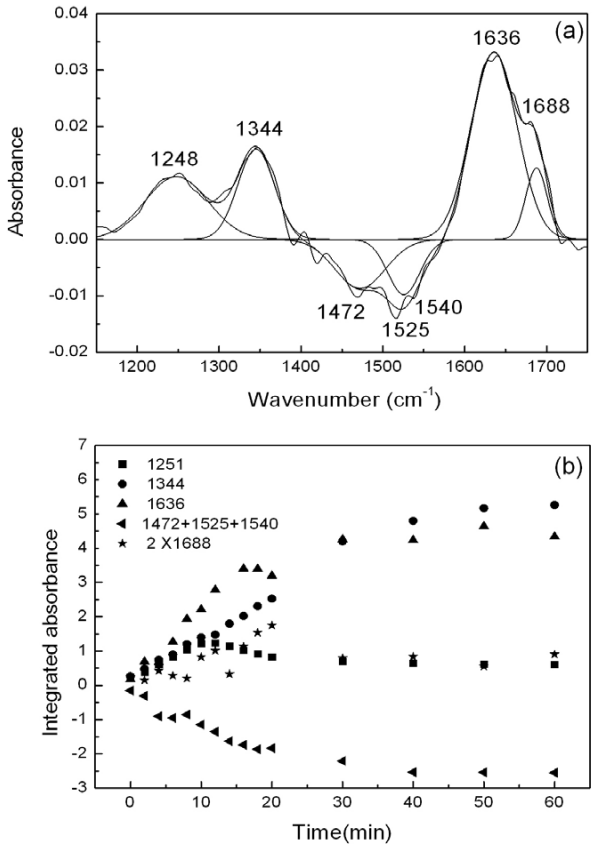

Fig. 7. **(a)** IR spectrum of $CaCO_3$ particles after reaction with 1.06×10^{16} molecules cm^{-3} of NO_2 for 60 min after Gaussian peak fitting. **(b)** Change in integrated absorbance of each peak with reaction time.

ACPD
9, 7115–7154, 2009

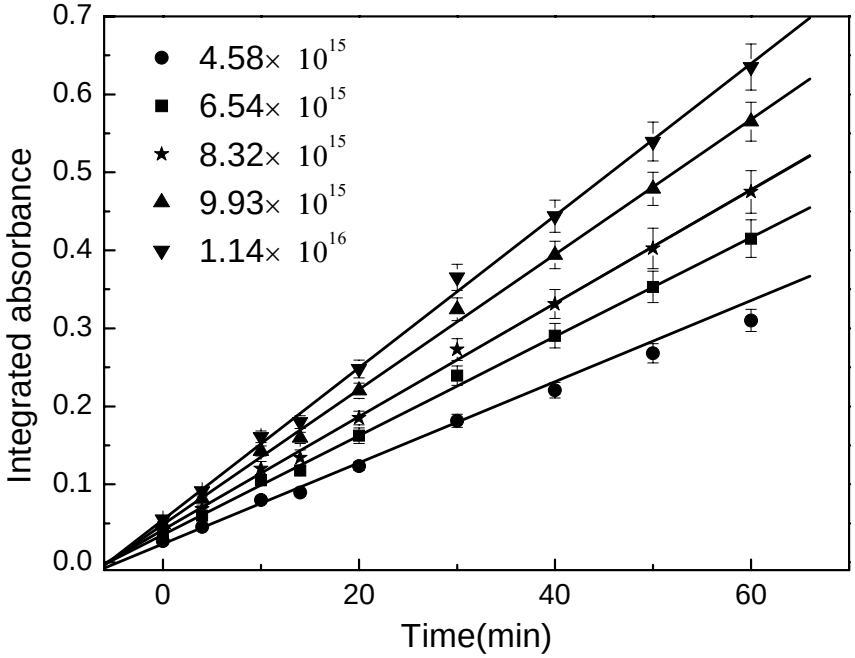

Fig. 8. Nitrate formation as a function of time during the reaction of $CaCO_3$ with NO_2 at 60–71%RH. The nitrate concentration is represented by the integrated absorbance of the peak area between 1077 and 1013 cm^{-1}. The NO_2 concentration was changed from 4.58×10^{15} to 1.14×10^{16} molecule cm^{-3}. The data points and the error bars are the average value and the standard deviation of three duplicate experiments.

ACPD
9, 7115–7154, 2009

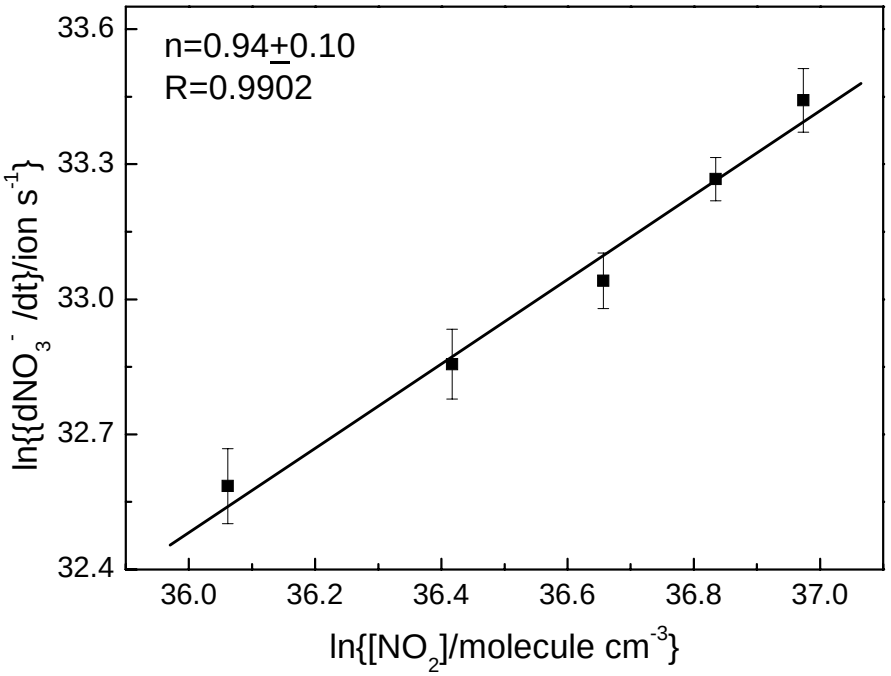

Fig. 9. Double-log plot of the nitrate production rate versus the NO_2 concentration. The reaction was at 296 K and RH=66±2%. The data points and error bars are the average values and standard deviations of two or three replicate experiments.

ACPD
9, 7115–7154, 2009

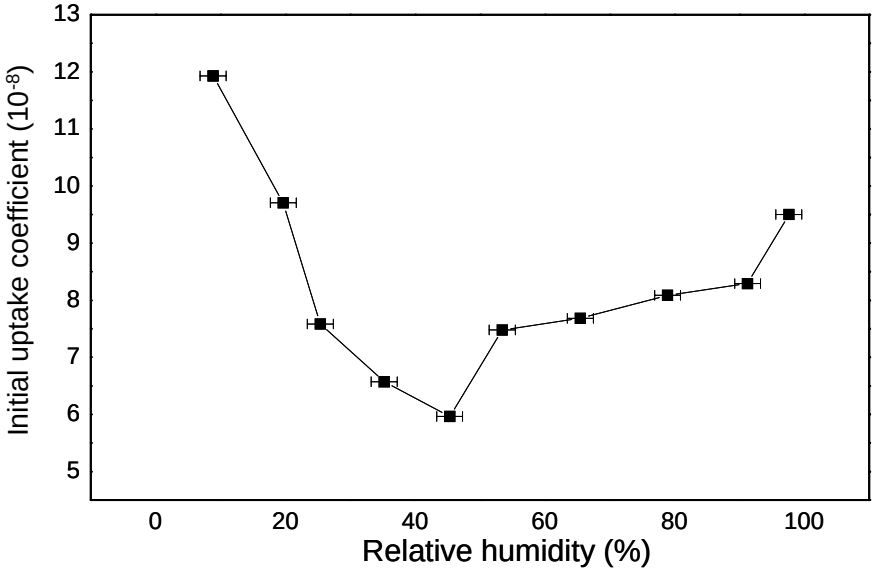

Fig. 10. Initial uptake coefficient of NO_2 on $CaCO_3$ at different RH, the NO_2 concentration was 6.88×10^{15} molecules cm^{-3} for uniform format. The horizontal error bars are the errors of RH measurements.

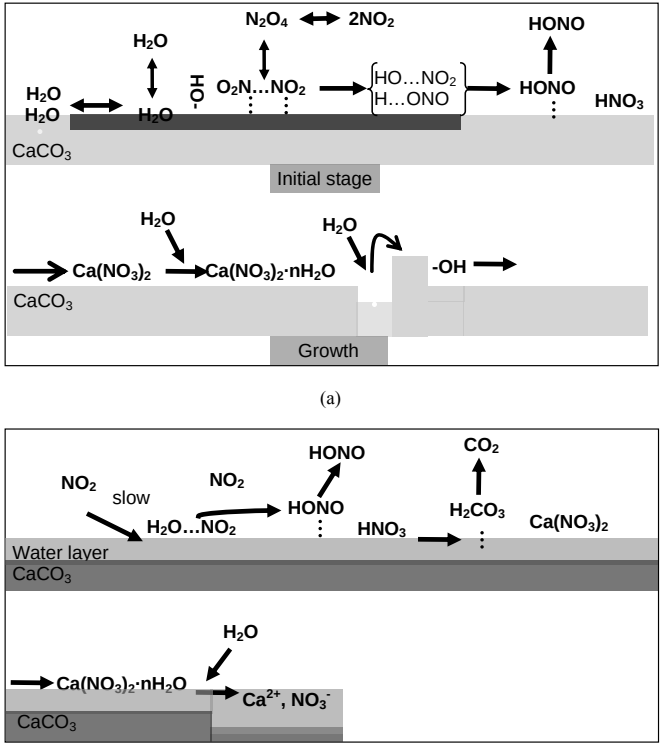

Fig. 11. Schematics of the mechanism of NO_2 reaction on the surface of $CaCO_3$ particles under **(a)** dry and **(b)** wet conditions.

ACPD
9, 7115–7154, 2009

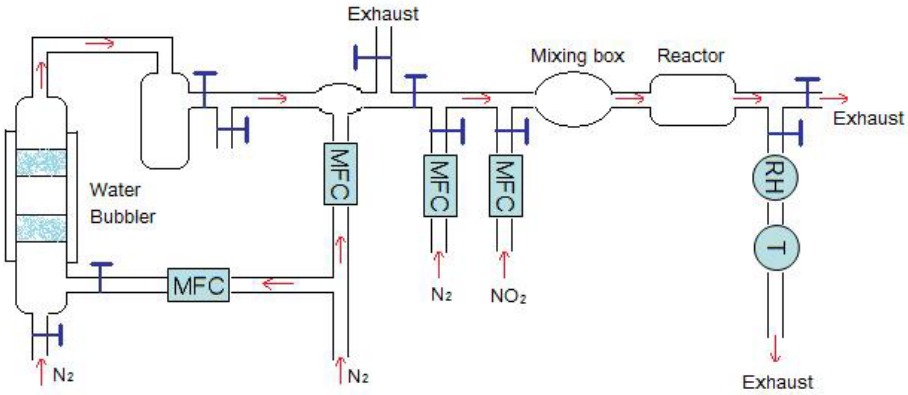

Fig. A1. Apparatus for gas preparation.

ACPD
9, 7115–7154, 2009

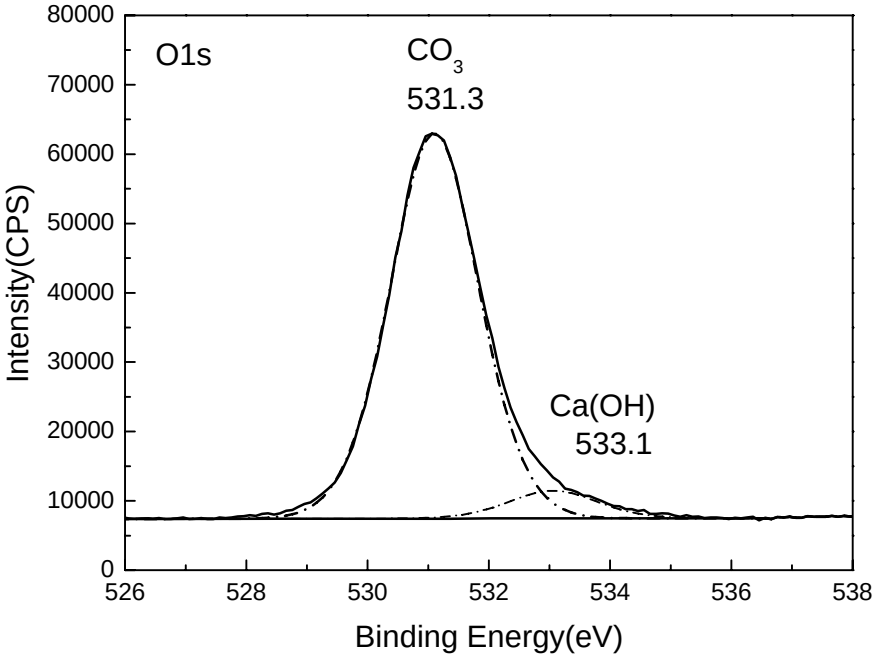

Fig. A2. XPS spectrum of O1s at the surface of $CaCO_3$ particles.

ACPD
9, 7115–7154, 2009

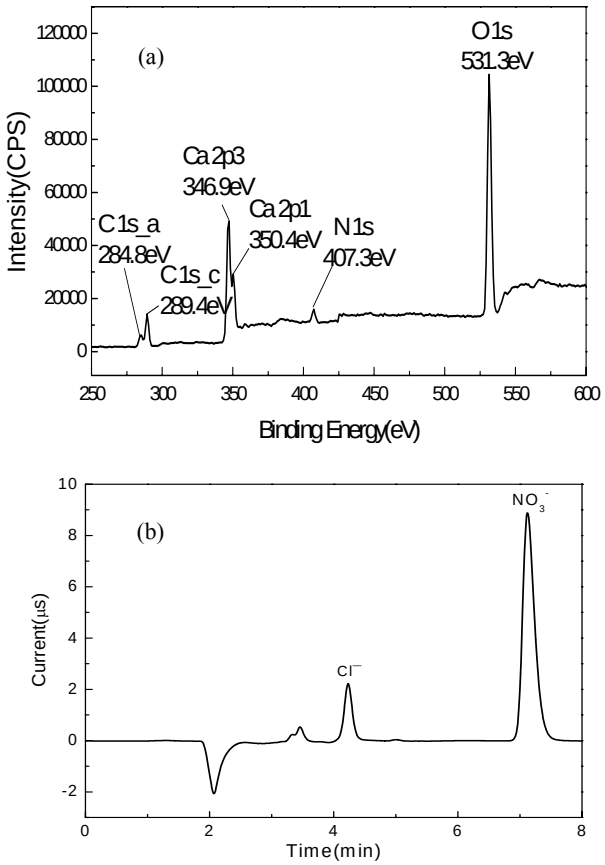

Fig. A3. Typical XPS spectrum **(a)** and IC chromatogram **(b)** of $CaCO_3$ particle after reacted with 1.06×10^{15} molecules cm^{-3} NO_2 for 626 min.

ACPD
9, 7115–7154, 2009

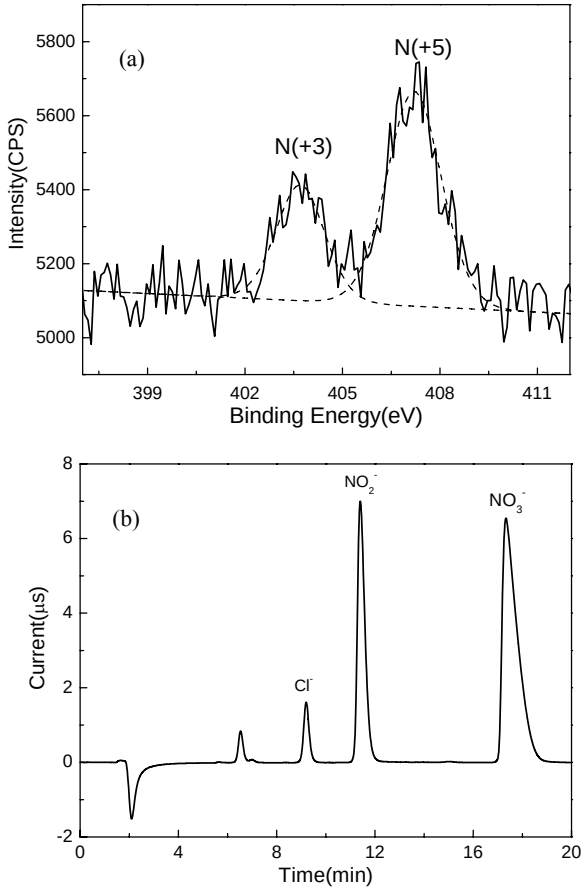

Fig. A4. XPS spectrum **(a)** and IC chromatogram **(b)** analysis of $CaCO_3$ particles after reaction with 1.06×10^{16} molecules cm^{-3} of NO_2 at RH=80±2% for 30 min. The dashed line in (a) was the Lorentzian peak fit.

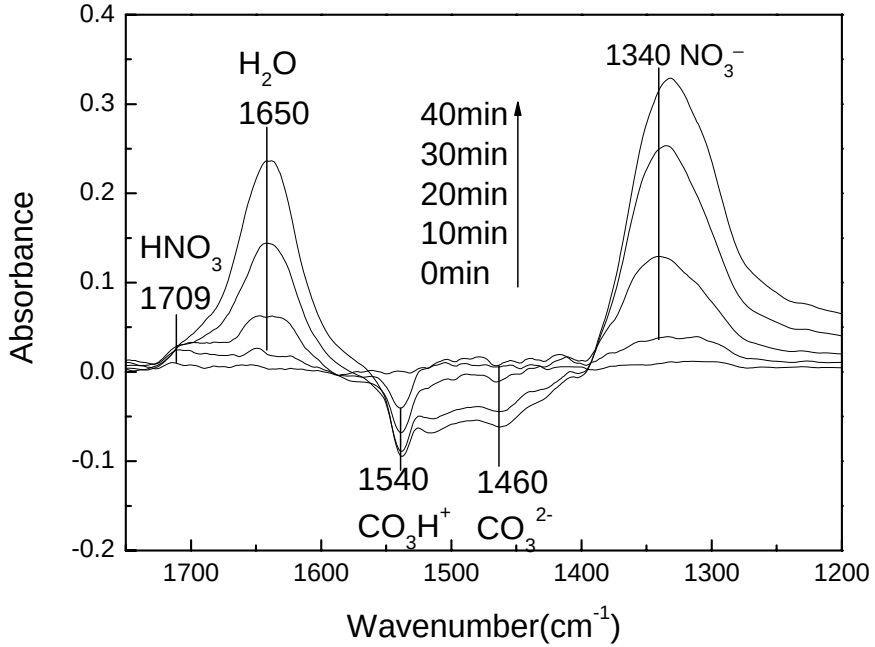

Fig. A5. Typical IR spectrum of $CaCO_3$ after reacted with HNO_3 for 0 to 40 min.

ACPD
9, 7115–7154, 2009